

Title	Tetrel bonding and other non-covalent interactions assisted supramolecular aggregation in a new Pb(II) complex of an isonicotinohydrazide
Authors	Mahmoudi, Ghodrat; Abedi, Marjan; Lawrence, Simon E.; Zangrando, Ennio; Babashkina, Maria G.; Klein, Axel; Frontera, Antonio; Safin, Damir A.
Publication date	2020-09-04
Original Citation	Mahmoudi, G., Abedi, M., Lawrence, S. E., Zangrando, E., Babashkina, M. G., Klein, A., Frontera, A. and Safin, D. A. (2020) 'Tetrel Bonding and Other Non-Covalent Interactions Assisted Supramolecular Aggregation in a New Pb(II) Complex of an Isonicotinohydrazide', <i>Molecules</i> , 25 (18), 4056, (15 pp). doi: 10.3390/molecules25184056
Type of publication	Article (peer-reviewed)
Link to publisher's version	<a href="https://www.mdpi.com/1420-3049/25/18/4056">https://www.mdpi.com/1420-3049/25/18/4056</a> - 10.3390/molecules25184056
Rights	© 2020 by the authors. Licensee MDPI, Basel, Switzerland. This article is an open access article distributed under the terms and conditions of the Creative Commons Attribution (CC BY) license - <a href="http://creativecommons.org/licenses/by/4.0/">http://creativecommons.org/licenses/by/4.0/</a>
Download date	2025-07-21 16:51:47
Item downloaded from	<a href="https://hdl.handle.net/10468/12439">https://hdl.handle.net/10468/12439</a>



# UCC

**University College Cork, Ireland**  
Coláiste na hOllscoile Corcaigh

## Article

# Tetrel Bonding and Other Non-Covalent Interactions Assisted Supramolecular Aggregation in a New Pb(II) Complex of an Isonicotinohydrazide

Ghodrat Mahmoudi <sup>1,\*</sup>, Marjan Abedi <sup>2</sup>, Simon E. Lawrence <sup>3</sup>, Ennio Zangrando <sup>4</sup>, Maria G. Babashkina <sup>5</sup>, Axel Klein <sup>5,\*</sup>, Antonio Frontera <sup>6</sup> and Damir A. Safin <sup>7,8,9,\*</sup>

<sup>1</sup> Department of Chemistry, Faculty of Science, University of Maragheh, Maragheh P.O. Box 55181-83111, Iran

<sup>2</sup> Department of Chemistry, Faculty of Science, University of Mohaghegh Ardabili, Ardabil P.O. Box 56199-11367, Iran; marjan\_abedi2004@yahoo.com

<sup>3</sup> School of Chemistry, Analytical and Biological Chemistry Research Facility, Synthesis and Solid State Pharmaceutical Centre, University College Cork, College Road, T12 K8AF Cork, Ireland; simon.lawrence@ucc.ie

<sup>4</sup> Department of Chemical and Pharmaceutical Sciences, University of Trieste, Via L. Giorgieri 1, 34127 Trieste, Italy; ezangrando@units.it

<sup>5</sup> Department für Chemie, Institut für Anorganische Chemie, Universität zu Köln, Greinstraße 6, D-50939 Köln, Germany; maria.babashkina@mail.ru

<sup>6</sup> Department of Chemistry, Universitat de les Illes Balears, Crta de Valldemossa km 5.7, 7122 Palma de Mallorca Balears, Spain; toni.frontera@uib.es

<sup>7</sup> Institute of Chemistry, University of Tyumen, Volodarskogo Str. 6, 625003 Tyumen, Russia

<sup>8</sup> West-Siberian Interregional Scientific and Educational Center, 625003 Tyumen, Russia

<sup>9</sup> Innovation Center for Chemical and Pharmaceutical Technologies, Ural Federal University named after the First President of Russia B.N. Eltsin, Mira Str. 19, 620002 Ekaterinburg, Russia

\* Correspondence: ghodratmahmoudi@gmail.com (G.M.); axel.klein@uni-koeln.de (A.K.); damir.a.safin@gmail.com (D.A.S.)

Received: 14 August 2020; Accepted: 2 September 2020; Published: 4 September 2020



**Abstract:** A new supramolecular Pb(II) complex  $[\text{PbL}(\text{NO}_2)]_n$  was synthesized from  $\text{Pb}(\text{NO}_3)_2$ ,  $N'$ -(1-(pyridin-2-yl)ethylidene)isonicotinohydrazide (**HL**) and  $\text{NaNO}_2$ .  $[\text{PbL}(\text{NO}_2)]_n$  is constructed from discrete  $[\text{PbL}(\text{NO}_2)]$  units with an almost ideal  $\text{N}_2\text{O}_3$  square pyramidal coordination environment around Pb(II). The ligand  $\text{L}^-$  is coordinated through the 2-pyridyl N-atom, one aza N-atom, and the carbonyl O-atom. The nitrite ligand binds in a  $\kappa^2\text{-O,O}$  coordination mode through both O-atoms. The Pb(II) center exhibits a hemidirected coordination geometry with a pronounced coordination gap, which allows a close approach of two additional N-atoms arising from the  $\text{N}=\text{C}(\text{O})$  N-atom of an adjacent molecule and from the 4-pyridyl N-atom from the another adjacent molecule, yielding a  $\text{N}_4\text{O}_3$  coordination, constructed from two Pb–N and three Pb–O covalent bonds, and two  $\text{Pb} \cdots \text{N}$  tetrel bonds. Dimeric units in the structure of  $[\text{PbL}(\text{NO}_2)]_n$  are formed by the  $\text{Pb} \cdots \text{N}=\text{C}(\text{O})$  tetrel bonds and intermolecular electrostatically enforced  $\pi^+ \cdots \pi^-$  stacking interactions between the 2- and 4-pyridyl rings and further stabilized by  $\text{C}-\text{H} \cdots \pi$  intermolecular interactions, formed by one of the methyl H-atoms and the 4-pyridyl ring. These dimers are embedded in a 2D network representing a simplified uninodal 3-connected **fes** (Shubnikov plane net) topology defined by the point symbol  $(4\cdot 8^2)$ . The Hirshfeld surface analysis of  $[\text{PbL}(\text{NO}_2)]$  revealed that the intermolecular  $\text{H} \cdots \text{X}$  ( $\text{X} = \text{H}, \text{C}, \text{N}, \text{O}$ ) contacts occupy an overwhelming majority of the molecular surface of the  $[\text{PbL}(\text{NO}_2)]$  coordination unit. Furthermore, the structure is characterized by intermolecular  $\text{C} \cdots \text{C}$  and  $\text{C} \cdots \text{N}$  interactions, corresponding to the intermolecular  $\pi \cdots \pi$  stacking interactions. Notably, intermolecular  $\text{Pb} \cdots \text{N}$  and, most interestingly,  $\text{Pb} \cdots \text{H}$  interactions are remarkable contributors to the molecular surface of  $[\text{PbL}(\text{NO}_2)]$ . While the former contacts are due to the  $\text{Pb} \cdots \text{N}$  tetrel bonds, the latter contacts are mainly due to the interaction with the methyl H-atoms in the  $\pi \cdots \pi$  stacked  $[\text{PbL}(\text{NO}_2)]$  molecules. Molecular electrostatic potential (MEP) surface calculations showed marked electrostatic contributions

to both the Pb $\cdots$ N tetrel bonds and the dimer forming  $\pi^+\cdots\pi^-$  stacking interactions. Quantum theory of atoms in molecules (QTAIM) analyses underlined the tetrel bonding character of the Pb $\cdots$ N interactions. The manifold non-covalent interactions found in this supramolecular assembly are the result of the proper combination of the polyfunctional multidentate pyridine-hydrazide ligand and the small nitrito auxiliary ligand.

**Keywords:** non-covalent interaction; tetrel bond; lead(II); isonicotinohydrazide; crystal structure; Hirshfeld surface analysis; DFT calculations

## 1. Introduction

Non-covalent interactions were first recognized by J. D. van der Waals in his doctoral thesis about one and a half century ago [1]. The most prominent example for the crucial role of non-covalent interactions is probably the double helix structure of DNA [2,3]. Different types of non-covalent interactions, such as hydrogen bonding,  $\pi\cdots\pi$  interaction, halogen bonding, chalcogen bonding, pnictogen bonding, tetrel bonding, (an)agostic bonding, and cation/anion $\cdots\pi$  interaction, can be distinguished, and their role in all areas of molecular chemistry and biology is eminent [3–23]. Amongst them, non-covalent  $\pi\cdots\pi$  interactions, also called  $\pi$ -stacking, found between aromatic systems, are of great interest due to their broad applications [4–11,13–16,18]. Moreover, «stacking interactions» can also be addressed to aliphatic systems [14]. Notably, benzene and cyclohexane interact more efficiently (−3.01 kcal/mol) [18] than benzene (−2.758 kcal/mol) [14] and cyclohexane (−2.62 kcal/mol) [7] dimers.

On the other hand, the coordination chemistry of Pb(II) gains particular interest from the large ionic radius of this heavy p-block metal ion, its rich variety of coordination numbers from 2 up to 10, and the peculiar feature of the 6s<sup>2</sup> lone-pair in the coordination sphere of its complexes [17,19,22,24–30]. This lone-pair can be stereochemically active, which is called hemidirectional or non-active, for which the term “holodirectional” was coined (Chart 1) [19,24–30]. The background is the observation that the electron pair on the Pb(II) atom is either stereochemically irrelevant (holodirected) or demanding space (hemidirected) [17,19].

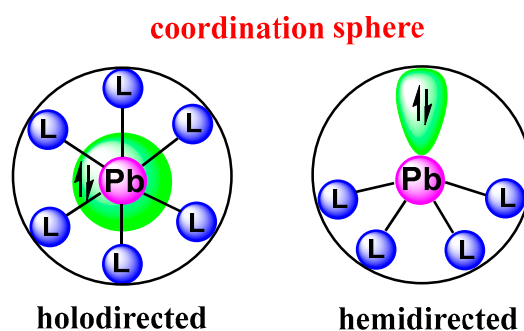
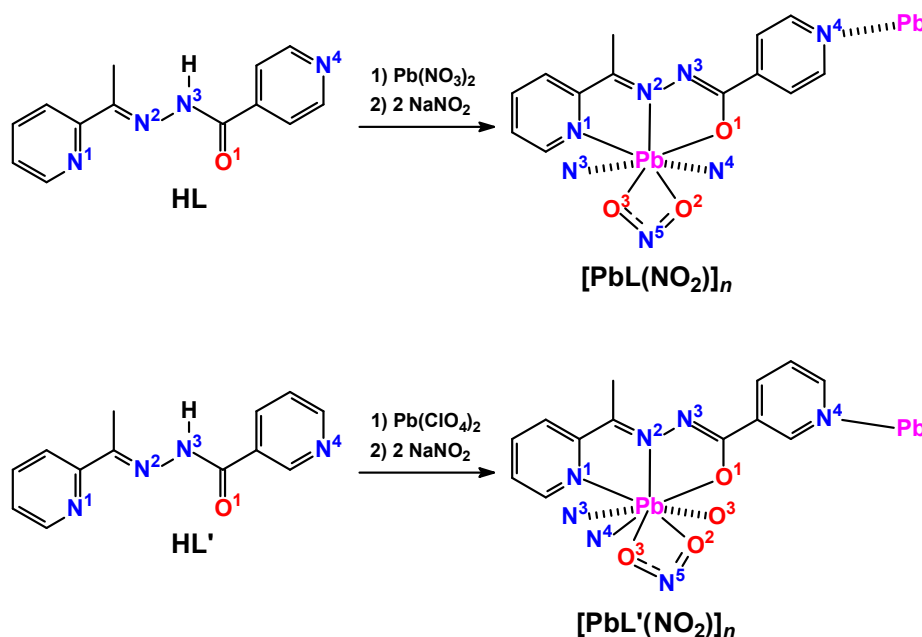


**Chart 1.** Simplified diagram for holodirected and hemidirected coordination spheres around Pb(II).

The hemidirected coordination allows Pb(II) to participate in the formation of tetrel bonds, which are of great importance for the resulting topology of Pb(II) coordination compounds [17,19,22,24–42]. Although the occurrence of hemidirected or holodirected bonding cannot be reliably predicted [19,28–31,40,41], recent work using polyfunctional multidentate ligands, such as carboxylates of 2-thiols or heterocycles [19,24–28], or the per se polyfunctional thiothiosemicarbazones, hydrazones, or Schiff base ligands of the salen or salan type [29–42] allowed formation of tetrel bonds. We also have recently contributed to this and have found the polyfunctional 1-(pyridin-2-yl)ethylideneisonicotinohydrazide ligand (**HL**, Scheme 1) extremely versatile to build up supramolecular Pb(II) complexes or

coordination polymers with rich non-covalent interactions, including the reliable formation of tetrel bonding [32,38,42]. Particularly, we have studied the heteroleptic complexes and coordination compounds of the type  $[\text{PbL}(\text{SCN})]_n$  and  $[\text{Pb}(\text{HL})(\text{NCS})_2]_n$  [32], and  $[\text{Pb}(\text{HL})\text{Cl}_2]_n$  [38]. From the isomeric 1-(pyridin-2-yl)ethylidenenicotinohydrazide ligand ( $\text{HL}'$ , Scheme 1) compounds of the type  $[\text{Pb}_2(\text{HL}')_2(\text{NO}_3)_2(\text{NCS})_2]$ ,  $[\text{PbL}'(\text{OAc})]_2$ ,  $\{[\text{Pb}(\text{HL}')(\text{OAc})]\text{ClO}_4\}_n$ ,  $\{[\text{PbL}']\text{ClO}_4\}_n \cdot n\text{H}_2\text{O}$ ,  $[\text{PbL}(\text{N}_3)]_n$  and  $[\text{PbL}'(\text{NO}_2)]_n$  [37], and  $[\text{Pb}(\text{HL}')(\text{NO}_3)_2]_n$  and  $[\text{PbL}'(\text{CH}_3\text{O})]_n$  [39] have been studied. We recently reported also the homoleptic complex  $[\text{Pb}(\text{L}'')]_2$  containing the  $\text{N}'$ -(4-hydroxybenzylidene)isonicotinohydrazide ligand [42].



**Scheme 1.** Syntheses of  $[\text{PbL}(\text{NO}_2)]_n$  (this work) and  $[\text{PbL}'(\text{NO}_2)]_n$  [37] (tetrel bonds shown as dashed lines).

In view of the interesting structure of the previously described nitrito nicotinohydrazide compound  $[\text{Pd}(\text{L}'(\text{NO}_2))]_n$  [37], we reacted a mixture of  $\text{Pb}(\text{NO}_3)_2$  and 1-(pyridin-2-yl)ethylideneisonicotinohydrazide (**HL**) with  $\text{NaNO}_2$  and received the corresponding isonicotino isomer  $[\text{PbL}(\text{NO}_2)]_n$ , which turned out to have a completely different structure compared with  $[\text{PbL}'(\text{NO}_2)]_n$  (Scheme 1). The nature and energetic features of the two  $\text{Pb} \cdots \text{N}$  tetrel bonds were studied by density functional theory (DFT) and molecular electrostatic potential (MEP) calculations, which demonstrate the presence of a  $\sigma$ -hole at the  $\text{Pb}(\text{II})$  ion.

## 2. Results and Discussion

The reaction of a mixture of  $\text{Pb}(\text{NO}_3)_2$  and **HL** with  $\text{NaNO}_2$  in MeOH led to a new supramolecular heteroleptic coordination compound  $[\text{PbL}(\text{NO}_2)]_n$  (Scheme 1). The compound was isolated as a crystalline air- and moisture-stable solid that was characterized through elemental analysis, FTIR spectroscopy, single-crystal X-ray diffraction, and Hirshfeld surface analysis.

The FTIR spectrum of  $[\text{PbL}(\text{NO}_2)]_n$  contains characteristic bands for the  $\text{C}=\text{O}$  and  $\text{C}=\text{N}$  bonds at 1632 and  $1590 \text{ cm}^{-1}$ , respectively. The methyl  $\text{C}-\text{H}$  fragments showed resonances at  $2921 \text{ cm}^{-1}$ .

Compound  $[\text{PbL}(\text{NO}_2)]_n$  crystallized in the monoclinic space group  $P2_1/n$ , with one coordination unit  $[\text{PbL}(\text{NO}_2)]$  in the asymmetric unit. The deprotonated  $\text{L}^-$  and the nitrito  $\text{NO}_2^-$  ligands were covalently bound to the metal center, yielding an almost ideal  $\text{N}_2\text{O}_3$  square pyramidal coordination environment around the  $\text{Pb}(\text{II})$  atom (Figure 1), as evidenced from the so-called  $\tau_5$ -descriptor of about 0.08 (Table 1) [43]. The ligand  $\text{L}^-$  is tridentately coordinated through the 2-pyridyl and the aza N-atoms and the carbonyl O-atom. The nitrite ligand binds in a  $\kappa^2\text{-O,O}$  coordination mode through both O-atoms to  $\text{Pb}(\text{II})$ .

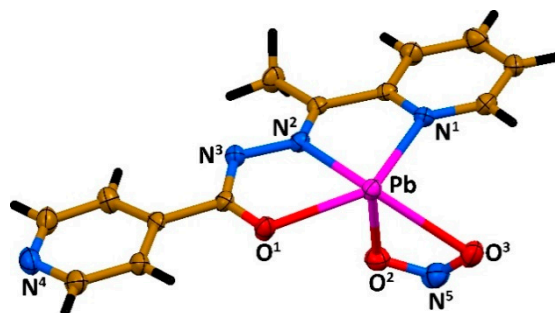


**Figure 1.** Molecular structure of the  $[\text{PbL}(\text{NO}_2)]$  unit in the structure of  $[\text{PbL}(\text{NO}_2)]_n$  (ellipsoids are drawn at 50% probability level). Color code: H = black, C = gold, N = blue, O = red, and Pb = magenta.

**Table 1.** Selected bond lengths (Å) and bond and torsion angles (°) in the structures of  $[\text{PbL}(\text{NO}_2)]_n$  and  $[\text{PbL}'(\text{NO}_2)]_n$  <sup>a</sup>.

	$[\text{PbL}(\text{NO}_2)]_n$ (This Work)	$[\text{PbL}'(\text{NO}_2)]_n$ [37]
Bond lengths (Å)		
Pb–N <sup>1</sup> (L/L')	2.583(4) (covalent)	2.535(5) (covalent)
Pb–N <sup>2</sup> (L/L')	2.462(4) (covalent)	2.452(4) (covalent)
Pb···N <sup>3</sup> (L/L')	3.235(4) (tetrel)	3.258(4) (tetrel)
Pb···N <sup>4</sup> (L/L')	3.039(5) (tetrel)	2.752(5) (covalent)
Pb–O <sup>1</sup> (L/L')	2.387(3) (covalent)	2.384(5) (covalent)
Pb–O <sup>2</sup> (NO <sub>2</sub> )	2.387(4) (covalent)	2.547(4) (covalent), 3.299(4) (tetrel)
Pb–O <sup>3</sup> (NO <sub>2</sub> )	2.768(4) (covalent)	2.904(5) (covalent)
Bond angles (°)		
O <sup>1</sup> –Pb–O <sup>2</sup>	82.35(13)	79.90(14)
O <sup>1</sup> –Pb–O <sup>3</sup>	124.07(13)	114.84(15)
O <sup>1</sup> –Pb–N <sup>1</sup>	128.82(12)	130.02(14)
O <sup>1</sup> –Pb–N <sup>2</sup>	65.50(12)	65.51(14)
O <sup>1</sup> –Pb–N <sup>4</sup>	–	91.30(14)
O <sup>2</sup> –Pb–O <sup>3</sup>	47.63(14)	44.26(14)
O <sup>2</sup> –Pb–N <sup>1</sup>	78.05(13)	81.12(14)
O <sup>2</sup> –Pb–N <sup>2</sup>	75.04(13)	70.61(14)
O <sup>2</sup> –Pb–N <sup>4</sup>	–	148.15(13)
O <sup>3</sup> –Pb–N <sup>1</sup>	70.93(12)	79.40(16)
O <sup>3</sup> –Pb–N <sup>2</sup>	112.30(13)	109.41(14)
O <sup>3</sup> –Pb–N <sup>4</sup>	–	153.72(15)
N <sup>1</sup> –Pb–N <sup>2</sup>	63.90(13)	64.62(14)
N <sup>1</sup> –Pb–N <sup>4</sup>	–	81.49(14)
N <sup>2</sup> –Pb–N <sup>4</sup>	–	77.86(13)
Torsion angles (°)		
2-Py···4/3-Py	3.5(3)	3.0(3)

<sup>a</sup> HL' = N'-(1-(pyridin-2-yl)ethylidene)nicotinohydrazide.

This structure is completely different from that of the previously reported nicotinohydrazide isomer  $[\text{PbL}'(\text{NO}_2)]_n$  [37]. In this coordination polymer, Pb(II) shows a distorted, non-octahedral six-fold coordination in which the pending 3-pyridyl N-atom bridges between two metals (Scheme 1 and Table 1).

The Pb–N bond lengths in  $[\text{PbL}(\text{NO}_2)]_n$  are 2.462(4) and 2.583(4) Å, with Pb–N(N) < Pb–N<sub>2-Py</sub>. The Pb–O distance with the carbonyl oxygen atom is shorter and of 2.387(3) Å. These values are in line with data from related hydrazide Pb(II) complexes [32,35,37–39,42]. The same bonds with the nitrite oxygen atoms differ significantly. Particularly, while one of the bonds has the same length as that

formed with the carbonyl O atom, the second bond with 2.768(4) Å is the longest within the covalent bonds formed by Pb(II) in the structure of  $[\text{PbL}(\text{NO}_2)]_n$ .

The covalent bond distances around the Pb(II) atom in  $[\text{PbL}(\text{NO}_2)]_n$  are very similar to the nicotinohydrazide isomer  $[\text{PbL}'(\text{NO}_2)]_n$  [37], and, in both cases, the corresponding organic ligand is almost completely planar, as can be seen from the torsion angles of only about 3° between the mean planes formed by the pyridyl rings (Table 1).

The covalent bonds in the central coordination unit are markedly concentrated on one hemisphere of the coordination environment (Figure 1), representing a hemidirected coordination geometry with a pronounced coordination gap, due to the  $6s^2$  lone pair. This allows for two additional N-atoms from adjacent molecules, the aza and the 4-pyridyl N-atoms, to approach the Pb(II) and form two  $\text{Pb} \cdots \text{N}$  tetrel bonds (Figure 2). The  $\text{Pb} \cdots \text{N}=\text{C}(\text{O})$  tetrel bond (3.235(4) Å) is significantly longer than the sum of the covalent radii (2.17 Å) and shorter than the sum of van der Waals radii (3.57 Å), thus supporting its non-covalent nature. It leads to the formation of centrosymmetric dimers  $[\text{PbL}(\text{NO}_2)]_2$  (Figure 2), which are further reinforced by bilateral  $\pi \cdots \pi$  stacking interactions, formed between the 2- and 4-pyridyl rings (Figure 2 and Table 2). These dimers are interlinked through bilateral  $\text{C}-\text{H} \cdots \pi$  intermolecular interactions, formed by one of the methyl H-atoms and the 4-pyridyl ring (Figure 2 and Table 3). The slightly shorter  $\text{Pb} \cdots \text{N}_{4\text{-Py}}$  tetrel bond (3.039(5) Å) leads to a supramolecular aggregation of the dimers into a 2D layer structure (Figure 3). From a topological perspective, this 2D metal–organic layer in  $[\text{PbL}(\text{NO}_2)]_n$  is assembled from the 3-connected Pb(II) nodes and 3-connected L linkers and can be classified as a uninodal 3-connected *fes* (Shubnikov plane net) [44] topology defined by the point symbol  $(4 \cdot 8^2)$ . Thus, the overall topology of  $[\text{PbL}(\text{NO}_2)]_n$  is a supramolecular 3D framework, formed by multiple non-covalent interactions, such as  $\text{Pb} \cdots \text{N}$  tetrel bonds,  $\pi \cdots \pi$  stacking, and  $\text{C}-\text{H} \cdots \pi$  interactions.

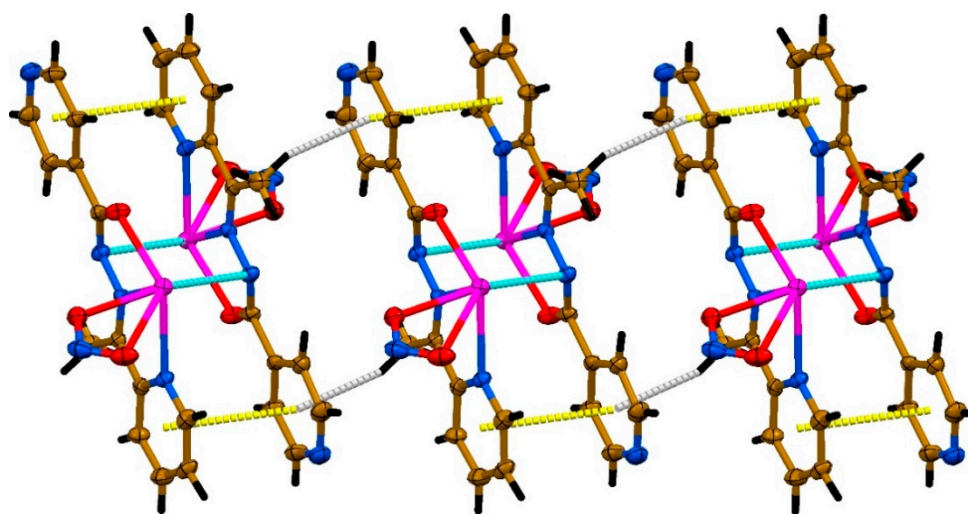


**Figure 2.** View on a 1D supramolecular chain in the structure of  $[\text{PbL}(\text{NO}_2)]_n$ , formed through  $\text{Pb} \cdots \text{N}=\text{C}(\text{O})$  tetrel bonds,  $\pi \cdots \pi$  stacking, and  $\text{C}-\text{H} \cdots \pi$  interactions (ellipsoids are drawn at 50% probability level). Color code: H = black, C = gold, N = blue, O = red, and Pb = magenta; cyan dashed line =  $\text{Pb} \cdots \text{N}$  tetrel bond, yellow dashed line =  $\pi \cdots \pi$  stacking interaction, and gray dashed line =  $\text{C}-\text{H} \cdots \pi$  interaction.



**Table 2.**  $\pi \cdots \pi$  inter-ring distances (Å) and angles (°) for  $[\text{PbL}(\text{NO}_2)]_n$  <sup>a</sup>.

Cg(I)	Cg(J)	$d[\text{Cg}(I) \cdots \text{Cg}(J)]$	$\alpha$	$\beta$	$\gamma$	Slippage	Symmetry Transformation
2-Py	4-Py	3.544(3)	3.5(3)	19.7	18.1	1.194	$2-x, 2-y, 1-z$
4-Py	2-Py	3.544(3)	3.5(3)	18.1	19.7	1.100	$2-x, 2-y, 1-z$

<sup>a</sup> Cg(I)  $\cdots$  Cg(J): distance between ring centroids of the 2-Py and 4-Py rings of the ligand L;  $\alpha$ : dihedral angle between planes Cg(I) and Cg(J);  $\beta$ : angle Cg(I)  $\rightarrow$  Cg(J) vector and normal to plane I;  $\gamma$ : angle Cg(I)  $\rightarrow$  Cg(J) vector and normal to plane J; slippage: distance between Cg(I) and perpendicular projection of Cg(J) on ring I.

**Table 3.** C–H  $\cdots \pi$  ring interactions distances (Å) and angles (°) for  $[\text{PbL}(\text{NO}_2)]_n$  <sup>a</sup>.

C–H(I)	$d[\text{C–H}(I)]$	Cg(J)	$d[\text{H}(I) \cdots \text{Cg}(J)]$	$d[\text{C} \cdots \text{Cg}(J)]$	$\angle [\text{CH}(I) \cdots \text{Cg}(J)]$	Symmetry Transformation
C7–H7B	0.98	4-Py	2.81	3.657(6)	145	$1-x, 2-y, 1-z$

<sup>a</sup> H(I)  $\cdots$  Cg(J): distance between the H(I) atom and ring centroid of the 4-Py ring of the ligand L; C  $\cdots$  Cg(J): distance between the C atom and ring centroid;  $[\text{CH}(I) \cdots \text{Cg}(J)]$ : angle between the bond C–H(I) and plane Cg(J).

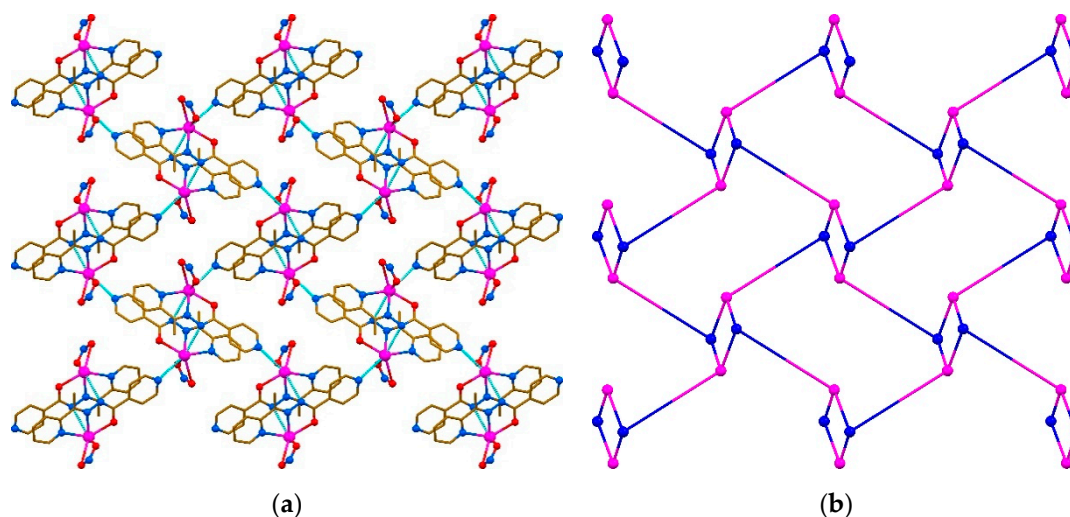


**Figure 3.** (a) View on the 2D supramolecular layer in the structure of  $[\text{PbL}(\text{NO}_2)]_n$ , formed through  $\text{Pb} \cdots \text{N}=\text{C}(\text{O})$  and  $\text{Pb} \cdots \text{N}_{4\text{-Py}}$  tetrel bonds (H-atoms were omitted for clarity). Color code: C = gold, N = blue, O = red, and Pb = magenta; cyan dashed line =  $\text{Pb} \cdots \text{N}$  tetrel bond. (b) Simplified underlying network of  $[\text{PbL}(\text{NO}_2)]_n$ , considering all  $\text{Pb} \cdots \text{N}$  tetrel bonds, with the uninodal 3-connected **fes** (Shubnikov plane net) topology defined by the point symbol of  $(4\cdot8^2)$ . Color code: Pb = magenta, and L = blue.

This stands in complete contrast to the previously reported nicotinohydrazide isomer  $[\text{PbL}'(\text{NO}_2)]_n$ , in which a similar  $\text{Pb} \cdots \text{N}=\text{C}(\text{O})$  tetrel bond and a very dissimilar  $\text{Pb} \cdots \text{ONO}$  tetrel bond lead to dimers, which are interconnected through the  $\text{Pb}-\text{N}_{3\text{-Py}}$  coordinative bond, thus forming a zigzag polymeric structure and only one remarkable  $\pi \cdots \pi$  stacking interaction with a centroid–centroid distance of 3.615(3) Å [37].

To further examine the intermolecular interactions in the crystal of  $[\text{PbL}(\text{NO}_2)]_n$ , we used a Hirshfeld surface analysis [45]. This analysis provides an excellent overview over all intermolecular interactions originating from a species, regardless of its nature. Together with the analysis of the nature of these interactions (XRD data, molecular electrostatic potential (MEP), binding energies from DFT, and quantum theory of atoms in molecules (QTAIM) calculations), it gives a complete picture, whose forces contribute to the molecular and crystal structure. The 2D fingerprint plots [46] of the basic coordination unit  $[\text{PbL}(\text{NO}_2)]$  were generated, using CrystalExplorer 3.1 [47], to visualize proportions of the intermolecular interactions. Furthermore, we calculated the enrichment ratios (*E*) [48] of the intermolecular contacts to estimate the probability of two chemical species to be in contact.

The Hirshfeld surface analysis showed that the intermolecular  $H\cdots X$  ( $X = H, C, N, O$ ) contacts occupy an overwhelming majority of the molecular surface of the basic coordination unit  $[PbL(NO_2)]$  (Figure 4 and Table 4). The shortest  $H\cdots H$  contacts are shown in the corresponding 2D fingerprint plot at  $d_e + d_i \approx 2.3 \text{ \AA}$ , and a clear splitting of the  $H\cdots H$  fingerprint was found (Figure 4), which is due to the shortest contact being between three atoms, rather than for a direct two-atom contact [45]. The  $H\cdots C$  contacts in the corresponding 2D plot of  $[PbL(NO_2)]$  were found in the form of «wings», with the shortest being  $d_e + d_i \approx 2.8 \text{ \AA}$  (Figure 4). This is characteristic for  $C-H\cdots\pi$  type of interactions [45]. The  $H\cdots N$  and  $H\cdots O$  contacts are shown in the corresponding 2D fingerprint plots as two «horns», with the shortest being  $d_e + d_i \approx 2.4\text{--}2.5 \text{ \AA}$  (Figure 4).

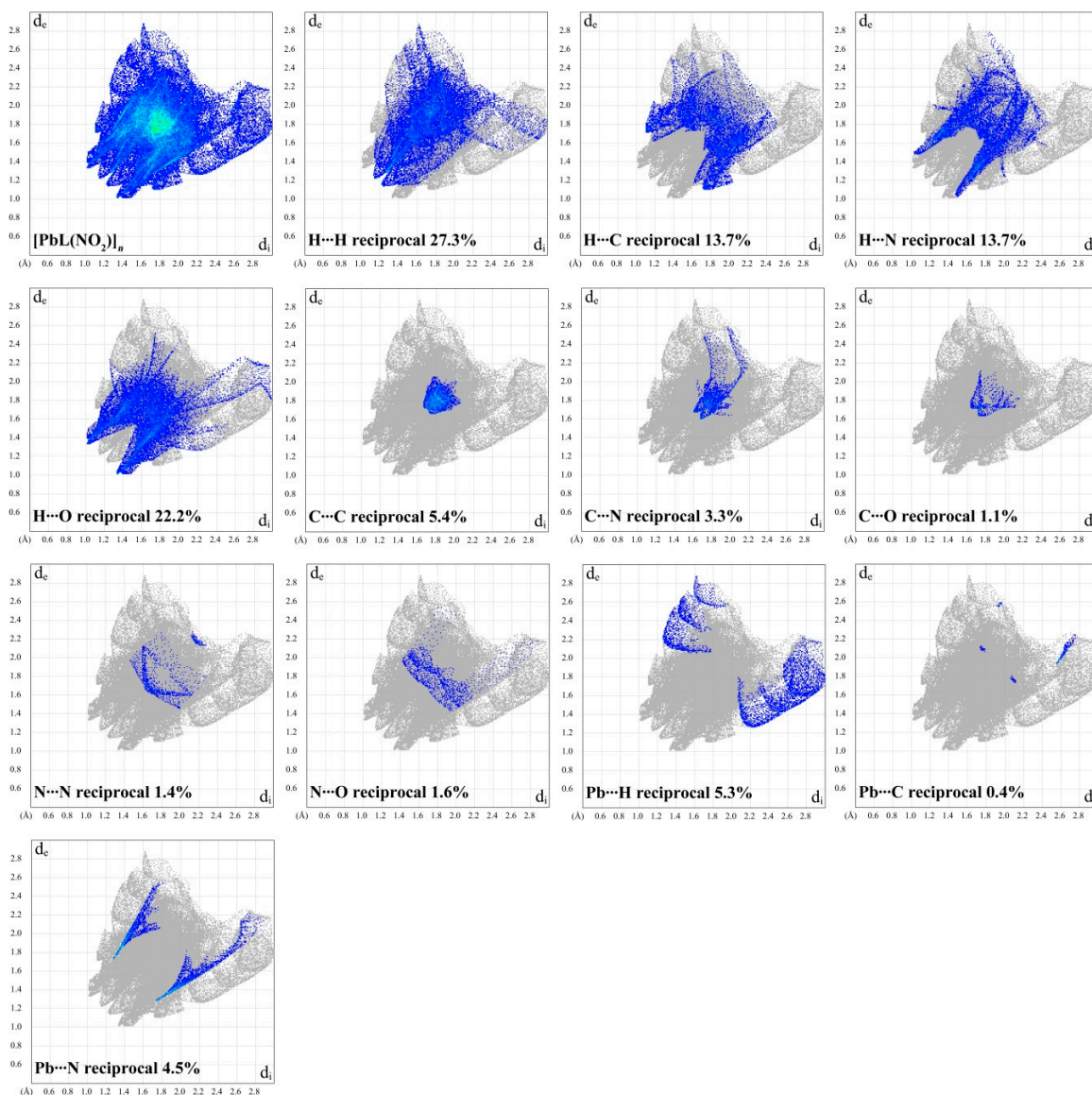


**Figure 4.** Two-dimensional and decomposed 2D fingerprint plots of observed contacts for  $[PbL(NO_2)]_n$ . The  $d_i$  value is the distance from the surface to the nearest atom interior to the surface, and  $d_e$  is the distance from the surface to the nearest atom exterior to the surface. Color code: blue = a fraction of the surface points of the corresponding contact.



**Table 4.** Hirshfeld contact surfaces and derived “random contacts” and “enrichment ratios” for  $[\text{PbL}(\text{NO}_2)]_n$  <sup>a</sup>.

	H	C	N	O	Pb
Contacts (C, %)					
H	27.3	–	–	–	–
C	13.7	5.4	–	–	–
N	13.7	3.3	1.4	–	–
O	22.2	1.1	1.6	0.0	–
Pb	5.3	0.4	4.5	0.0	0.0
Surface (S, %)					
	54.8	14.7	13.0	12.5	5.1
Random contacts (R, %)					
H	30.0	–	–	–	–
C	16.1	2.2	–	–	–
N	14.2	3.8	1.7	–	–
O	13.7	3.7	3.3	1.6	–
Pb	5.6	1.5	1.3	1.3	0.3
Enrichment (E) <sup>b</sup>					
H	0.91	–	–	–	–
C	0.85	2.45	–	–	–
N	0.96	0.87	0.82	–	–
O	1.62	0.30	0.48	0.00	–
Pb	0.95	0.27	3.46	0.00	–

<sup>a</sup> Values were obtained by using CrystalExplorer 3.1 [47]. <sup>b</sup> The “enrichment ratios” were not computed when the “random contacts” were lower than 0.9%, as they are not meaningful [48].

Furthermore, the structure of  $[\text{PbL}(\text{NO}_2)]$  is also characterized through intermolecular C⋯C and C⋯N interactions (Figure 4) observed as the area at  $d_e = d_i \approx 1.7\text{--}2.0$  Å. They correspond to intermolecular  $\pi \cdots \pi$  stacking interactions between the pyridyl rings. Importantly, intermolecular Pb⋯N and, most interestingly, Pb⋯H interactions are also remarkable contributors into the molecular surface of  $[\text{PbL}(\text{NO}_2)]$ . The former contacts are shown in the corresponding 2D fingerprint plot as two sharp «spikes», with the shortest being  $d_e + d_i \approx 3.0$  Å (Figure 4), and correspond to the Pb⋯N tetrel bonds. The latter contacts are mainly due to the interaction with the methyl H-atoms arising from an adjacent  $\pi \cdots \pi$  stacked  $[\text{PbL}(\text{NO}_2)]$  unit.

The 2D plot of  $[\text{PbL}(\text{NO}_2)]$  exhibits points at large  $d_e$  and  $d_i$  (Figure 4), which are similar to those observed in the 2D plots of benzene [45] and have been observed in similar compounds [49–54]. They correspond to regions without any close contacts to adjacent molecules.

The favorable H⋯X (X = H, N, O, Pb) contacts in the structure of  $[\text{PbL}(\text{NO}_2)]_n$  show enrichment ratios  $E_{\text{HH}/\text{HN}/\text{HO}/\text{PbH}}$  close to or even higher than unity (Table 4). The H⋯C, C⋯N, and N⋯N contacts are much less favored, and they are consistent with smaller enrichment ratios of  $E_{\text{HC}/\text{CN}/\text{NN}} = 0.82\text{--}0.87$ . This is explained by the presence of the highly probable C⋯C ( $E_{\text{CC}} = 2.45$ ) and Pb⋯N ( $E_{\text{PbN}} = 3.46$ ) contacts in the structure of the compound. Remaining contacts are discouraged with enrichment ratios ranging from 0.00 to 0.48 (Table 4).

As the Pb⋯N=C(O) tetrel bonding and the  $\pi \cdots \pi$  stacking interactions are the dominating forces for the formation of the dimers in the solid state of  $[\text{PbL}(\text{NO}_2)]_n$  (Figures 2 and 3), we further analyzed the donor–acceptor properties of the basic coordination unit  $[\text{PbL}(\text{NO}_2)]$  through DFT calculations.

First, we computed the molecular electrostatic potential (MEP) surface and found the highest positive values at the Pb(II) atom (+26.7 kcal/mol) representing the  $\sigma$ -hole (Figure 5). The most negative part is located at the 4-pyridyl N-atom (−40.8 kcal/mol) of the ligand  $\text{L}^-$ , which is more electron-rich than the nitrito N- and O-atoms (−31.4, −33.3, and −37.6 kcal/mol). Consequently, the Pb⋯N<sub>4-Py</sub> tetrel bonding interaction is the most favored contact from an electrostatic point of view in line with the

observed structure,  $d(\text{Pb} \cdots \text{N}_{4\text{-Py}}) = 3.039(5) \text{ \AA}$  (Table 1). The second  $\text{Pb} \cdots \text{N}=\text{C}(\text{O})$  tetrel bond is much weaker ( $3.235(4) \text{ \AA}$ ) and consistent with a significantly less negative value at the  $\text{N}=\text{C}(\text{O})$  N-atom ( $-21.3 \text{ kcal/mol}$ ). From these MEP calculations, a relatively high probability of a  $\text{Pb} \cdots \text{ONO}$  tetrel bond can be concluded. However, no such bond was observed in the structure of  $[\text{PbL}(\text{NO}_2)]_n$ . In contrast to this, in the nicotinohydrazide isomer  $[\text{PbL}'(\text{NO}_2)]_n$ , such a  $\text{Pb} \cdots \text{ONO}$  tetrel bond was observed, although not very dominant and rather long ( $3.299(4) \text{ \AA}$ , Table 1).

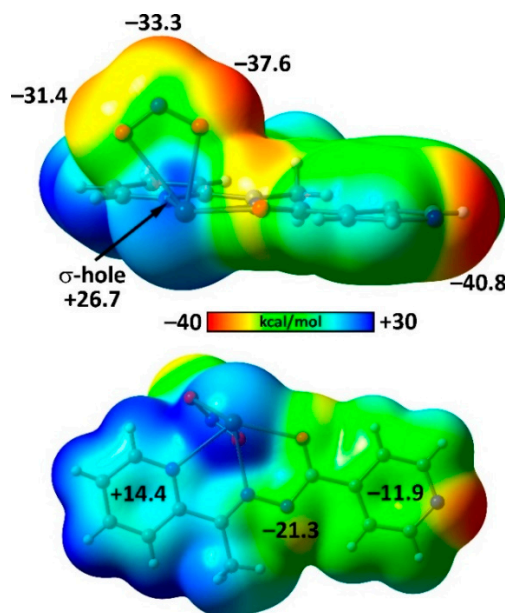


**Figure 5.** Two views of the molecular electrostatic potential (MEP) surface of  $[\text{PbL}(\text{NO}_2)]_n$  (isosurface  $0.001 \text{ a.u.}$ ). The blue color is used for positive MEP values, and the red color for negative values, as indicated in the legend.

An interesting feature of the surface is that the MEP values over the coordinated and non-coordinated pyridine ring centers represent opposite signs (Figure 5). As a consequence, they are well suited to form strong, electrostatically enforced  $\pi^+ \cdots \pi^-$  interactions [6] between the coordinated and non-coordinated pyridine rings of the  $\text{L}^-$  ligand, in line with the dimer-promoting stacking interactions found in  $[\text{PbL}(\text{NO}_2)]_n$  (Figure 2 and Table 2).

The DFT-calculated binding energy of these antiparallel stacked dimers composed of electrostatically enforced  $\pi^+ \cdots \pi^-$  and  $\text{Pb} \cdots \text{N}=\text{C}(\text{O})$  tetrel interactions (Figure 6) is quite large ( $\Delta E_1 = -24.3 \text{ kcal/mol}$ ), in agreement with the MEP surface analysis. In contrast to this, the calculated interaction energy of the  $\text{Pb} \cdots \text{N}_{4\text{-Py}}$  tetrel bond is moderately strong ( $\Delta E_2 = -10.2 \text{ kcal/mol}$ ) and comparable to recently reported values [32,35]. When looking at the bond (red spheres), ring (yellow spheres), and cage (blue spheres) critical points (CPs), we found that the  $\pi^+ \cdots \pi^-$  interaction is characterized by two bond CPs that interconnect two atoms of each pyridine ring (Figure 6). The  $\pi \cdots \pi$  stacking is further characterized by additional CPs that interconnect the chelate rings and more ring and cage CPs. Moreover, the two  $\text{Pb} \cdots \text{N}=\text{C}(\text{O})$  tetrel bonds are characterized by bond CPs and bond paths (Figure 6). The  $\text{Pb} \cdots \text{N}_{4\text{-Py}}$  tetrel bond contributes, together with a  $\text{C}-\text{H} \cdots \text{O}$  interaction, to the overall binding energy of entire assembly (Figure 6). The energy associated to this  $\text{C}-\text{H} \cdots \text{O}$  interaction was estimated by using the kinetic energy density predictor ( $E = 0.5 \times \text{Vr}$ ) to  $1.3 \text{ kcal/mol}$ . The  $\text{Pb} \cdots \text{N}_{4\text{-Py}}$  tetrel bond interaction is thus significantly stronger in keeping with the quite short experimentally observed distance of  $3.039(5) \text{ \AA}$ . Thus, this tetrel bond dominates this type of intermolecular interaction and drives the formation of the uninodal 3-connected *fes* (Shubnikov plane net) topology.

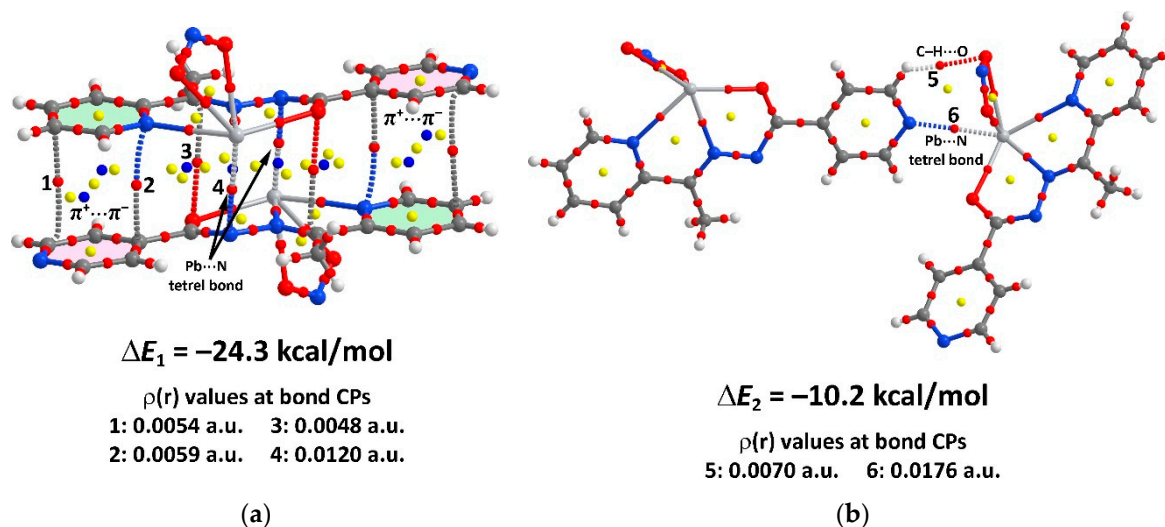


**Figure 6.** Quantum theory of atoms in molecules (QTAIM) analysis of (a) the antiparallel stacking dimer in  $[\text{PbL}(\text{NO}_2)]_n$  as a combination of the  $\text{Pb} \cdots \text{N}=\text{C}(\text{O})$  tetrel bonds and  $\pi^+ \cdots \pi^-$  interactions and (b) of two basic coordination units in  $[\text{PbL}(\text{NO}_2)]_n$  forming a  $\text{Pb} \cdots \text{N}_{4\text{-Py}}$  tetrel bond and  $\text{C}-\text{H} \cdots \text{O}$  bridging interaction. Bond, ring, and cage critical points are represented by red, yellow, and blue spheres, respectively. Bond paths connecting bond critical points are represented by dashed lines.  $\Delta E$  = accumulated dimerization energies.  $\rho(r)$  = densities at the bond critical points.

### 3. Materials and Methods

#### 3.1. Reagents

All reactants were used as received, without further purification. The ligand **HL** was synthesized by following the available protocol [37].

#### 3.2. Instrumentation

FTIR spectra were recorded on a Bruker Tensor 27 FTIR spectrometer (Bruker, Ettlingen, Germany). Microanalyses were performed, using a Heraeus CHN-O-Rapid analyzer (Heraeus, Hanau, Germany).

#### 3.3. Synthesis of $[\text{PbL}(\text{NO}_2)]_n$

A solution of **HL** (0.024 g, 0.1 mmol) in MeOH (10 mL) was added dropwise to a solution of  $\text{Pb}(\text{NO}_3)_2$  (0.033 g, 0.1 mmol), in the same solvent (10 mL). To this mixture, a solution of  $\text{NaNO}_2$  (0.014 g, 0.2 mmol) in MeOH (5 mL) was added slowly under stirring. The resulting mixture was stirred at room temperature for 30 min and was left undisturbed for slow evaporation. After about 4 days, yellow X-ray suitable single crystals were formed. Crystals were isolated by filtration. Yield: 0.038 g (78% based on  $\text{Pb}(\text{NO}_3)_2$ ). FTIR,  $\nu$ : 2921 (CH), 1632 (C=O), 1590 (C=N), 1269 ( $\text{NO}_2$ )  $\text{cm}^{-1}$ . *Anal.* Calc. for  $\text{C}_{13}\text{H}_{11}\text{N}_5\text{O}_3\text{Pb}$  (492.46): C 31.71, H 2.25, and N 14.22; found: C 31.80, H 2.28, and N 14.18%.

#### 3.4. Single-Crystal X-Ray Diffraction of $[\text{PbL}(\text{NO}_2)]_n$

The data were collected with a Bruker AXS SMART APEX2 CCD (Bruker, Ettlingen, Germany) diffractometer, operating at 179(2) K and using graphite monochromated Mo- $\text{K}\alpha$  radiation ( $\lambda = 0.71073 \text{ \AA}$ ). Cell refinement, indexing, and scaling of the datasets were performed, using the program Bruker Smart Apex and Saint packages [55]. The structure was solved by direct methods and refined by full-matrix least-squares on  $F^2$  with anisotropic displacement parameters for all non-hydrogen atoms, using the program SHELXL [56]. The H atoms were included as riding contributions with fixed isotropic displacement parameters in idealized positions. All the calculations were carried out by using the WinGX System, V2013.3 [57]. Crystal structure determination and refinement data are given in Table 5. CCDC-2014301 contains the supplementary crystallographic

data for this paper (Supplementary Materials). These data can be obtained free of charge via <http://www.ccdc.cam.ac.uk/conts/retrieving.html> (or from the CCDC, 12 Union Road, Cambridge CB2 1EZ, UK; Fax: +44 1223 336033; E-mail: deposit@ccdc.cam.ac.uk).

**Table 5.** Crystallographic data for  $[\text{PbL}(\text{NO}_2)]_n$ .

Parameter	$[\text{PbL}(\text{NO}_2)]_n$
Chemical formula	$\text{C}_{13}\text{H}_{11}\text{N}_5\text{O}_3\text{Pb}$
Formula weight	492.46
Crystal system	monoclinic
Space group	$P2_1/n$
$a$ (Å)	8.1660(11)
$b$ (Å)	13.2850(17)
$c$ (Å)	13.7842(18)
$\beta$ (°)	92.860(4)
$V$ (Å <sup>3</sup> )	1493.5(3)
$Z$	4
$D_{\text{calc}}$ (g/cm <sup>3</sup> )	2.190
$\mu(\text{Mo-K}\alpha)$ (mm <sup>−1</sup> )	11.316
$F(000)$	920
$\theta$ range (°)	2.13–27.32
Reflections collected	18486
No. of unique data	3318
$R_{\text{int}}$	0.0505
Observed data [ $I > 2\sigma(I)$ ]	2666
Parameters refined	200
Goodness of fit ( $F^2$ )	1.033
$R_1$ [ $I > 2\sigma(I)$ ] <sup>1</sup>	0.0288
$wR_2$ [ $I > 2\sigma(I)$ ] <sup>2</sup>	0.0625

$$^1 R_1 = \Sigma(|F_o| - |F_c|)/\Sigma|F_o|, ^2 wR_2 = [\Sigma w(F_o^2 - F_c^2)^2/\Sigma w F_o^2]^2]^{1/2}.$$

### 3.5. DFT Calculations

Gaussian-16 package [58] was used to perform the density functional theory calculations reported herein. In particular, the PBE1PBE-D3 functional [59,60], in combination with the def2-TZVP basis set [61,62], was employed for computing the binding energies and the molecular electrostatic potential (MEP) surfaces. The crystallographic coordinates were used for the calculations. The 0.001 a.u. isosurface was used for mapping the MEP onto the van der Waals surface. The QTAIM analysis [63] was carried out at the same level of theory and using the program AIMAll [64].

## 4. Conclusions

A new supramolecular Pb(II) coordination compound  $[\text{PbL}(\text{NO}_2)]_n$  was synthesized through treating a mixture of  $\text{Pb}(\text{NO}_3)_2$  and  $N'$ -(1-(pyridin-2-yl)ethylidene)isonicotinohydrazide (**HL**) with  $\text{NaNO}_2$ . The yellow material is composed of discrete mononuclear heteroleptic  $[\text{PbL}(\text{NO}_2)]$  coordination units containing the tridentate  $\text{N}^+\text{N}^+\text{O}$  binding deprotonated ligand  $\text{L}^-$  and a  $\kappa^2\text{-O,O}$  binding nitrito  $\text{NO}_2^-$  ligand. Pb(II) exhibits a hemidirected coordination geometry with a pronounced coordination gap. This allows two  $\text{Pb} \cdots \text{N}=\text{C}(\text{O})$  tetrel bonds of the uncoordinated N-atoms of two symmetry related  $[\text{PbL}(\text{NO}_2)]$  molecules forming pronounced dimers in the crystal and  $\text{Pb} \cdots \text{N}_{4\text{-Py}}$  tetrel bonds to the pending 4-pyridyl group forming a 2D network representing a simplified uninodal 3-connected **fes** (Shubnikov plane net) topology defined by the point symbol  $(4\cdot 8^2)$ . Thus, Pb(II) is in a  $\text{N}_4\text{O}_3$  coordination environment, formed by two covalent Pb–N, three covalent Pb–O bonds, and two  $\text{Pb} \cdots \text{N}$  tetrel bonds. The  $\text{Pb} \cdots \text{N}$  tetrel bonds in the crystal packing of  $[\text{PbL}(\text{NO}_2)]_n$  are further reinforced by bilateral intermolecular  $\pi \cdots \pi$  stacking interactions, formed between the 2- and 4-p.

**Supplementary Materials:** The following are available online. The cif and checkcif files.

**Author Contributions:** Conceptualization, G.M. and D.A.S.; methodology, M.A.; software, S.E.L., E.Z., and A.F.; investigation, all authors; resources, M.A. and A.K.; data curation, E.Z.; writing—original draft preparation, D.A.S., A.F., and M.G.B.; writing—review and editing, D.A.S., M.G.B., and A.K.; visualization, D.A.S. and A.K.; supervision, G.M.; project administration, G.M. and D.A.S. All authors have read and agreed to the published version of the manuscript.

**Funding:** This research was funded by the MICIU/AEI of Spain (project CTQ2017-85821-R FEDER funds) and by the Science Foundation Ireland, under grant no. 05/PICA/B802/EC07.

**Acknowledgments:** G.M. thanks the University of Maragheh for the financial support of this research.

**Conflicts of Interest:** The authors declare no conflict of interest.

## References

1. Van der Waals, J.D. Over de Continuïteit van den Gas-en Vloiestoestand. Ph.D. Thesis, University of Leiden, Leiden, The Netherlands, 1873.
2. Watson, J.D.; Crick, F.H.C. Molecular Structure of Nucleic Acids: A Structure for Deoxyribose Nucleic Acid. *Nature* **1953**, *171*, 737–738. [[CrossRef](#)] [[PubMed](#)]
3. Scheiner, S. New ideas from old concepts: The hydrogen bond. *Biochemist* **2019**, *41*, 6–9. [[CrossRef](#)]
4. Hobza, P.; Zahradník, R. Intermolecular Interactions between Medium-Sized Systems. Nonempirical and Empirical Calculations of Interaction Energies: Successes and Failures. *Chem. Rev.* **1988**, *88*, 871–897. [[CrossRef](#)]
5. Müller-Dethlefs, K.; Hobza, P. Noncovalent Interactions: A Challenge for Experiment and Theory. *Chem. Rev.* **2000**, *100*, 143–168. [[CrossRef](#)]
6. Janiak, C. A critical account on  $\pi$ – $\pi$  stacking in metal complexes with aromatic nitrogen-containing ligands. *J. Chem. Soc. Dalton Trans.* **2000**, 3885–3896. [[CrossRef](#)]
7. Ran, J.; Wong, M.W. Saturated Hydrocarbon–Benzene Complexes: Theoretical Study of Cooperative CH/ $\pi$  Interactions. *J. Phys. Chem. A* **2006**, *110*, 9702–9709. [[CrossRef](#)]
8. Hobza, P.; Zahradník, R.; Müller-Dethlefs, K. The World of Non-Covalent Interactions: 2006. *Collect. Czech. Chem. Commun.* **2006**, *71*, 443–531. [[CrossRef](#)]
9. Riley, K.E.; Pitoňák, M.; Jurečka, P.; Hobza, P. Stabilization and Structure Calculations for Noncovalent Interactions in Extended Molecular Systems Based on Wave Function and Density Functional Theories. *Chem. Rev.* **2010**, *110*, 5023–5063. [[CrossRef](#)]
10. Kim, K.S.; Karthikeyan, S.; Singh, N.J. How Different Are Aromatic  $\pi$  Interactions from Aliphatic  $\pi$  Interactions and Non- $\pi$  Stacking Interactions? *J. Chem. Theory Comput.* **2011**, *7*, 3471–3477. [[CrossRef](#)]
11. Salonen, L.M.; Ellermann, M.; Diederich, F. Aromatic Rings in Chemical and Biological Recognition: Energetics and Structures. *Angew. Chem. Int. Ed.* **2011**, *50*, 4808–4842. [[CrossRef](#)]
12. Riley, K.E.; Hobza, P. On the Importance and Origin of Aromatic Interactions in Chemistry and Biodisciplines. *Acc. Chem. Res.* **2013**, *46*, 927–936. [[CrossRef](#)] [[PubMed](#)]
13. Wheeler, S.E. Understanding Substituent Effects in Noncovalent Interactions Involving Aromatic Rings. *Acc. Chem. Res.* **2013**, *46*, 1029–1038. [[CrossRef](#)] [[PubMed](#)]
14. Mahadevi, A.S.; Sastry, G.N. Cooperativity in Noncovalent Interactions. *Chem. Rev.* **2016**, *116*, 2775–2825. [[CrossRef](#)] [[PubMed](#)]
15. Řezáč, J.; Hobza, P. Benchmark Calculations of Interaction Energies in Noncovalent Complexes and Their Applications. *Chem. Rev.* **2016**, *116*, 5038–5071. [[CrossRef](#)]
16. Biedermann, F.; Schneider, H.-J. Experimental Binding Energies in Supramolecular Complexes. *Chem. Rev.* **2016**, *116*, 5216–5300. [[CrossRef](#)]
17. Bauzá, A.; Mooibroek, T.J.; Frontera, A. Tetrel Bonding Interactions. *Chem. Rev.* **2016**, *16*, 473–487. [[CrossRef](#)]
18. Thakuria, R.; Nath, N.K.; Saha, B.K. The Nature and Applications of  $\pi$ – $\pi$  Interactions: A Perspective. *Cryst. Growth Des.* **2019**, *19*, 523–528. [[CrossRef](#)]
19. Bauzá, A.; Seth, S.K.; Frontera, A. Tetrel bonding interactions at work: Impact on tin and lead coordination compounds. *Coord. Chem. Rev.* **2019**, *384*, 107–125. [[CrossRef](#)]
20. Silvi, B.; Alikhani, E.; Ratajczak, H. Towards an unified chemical model of secondary bonding. *J. Mol. Model.* **2020**, *26*, 62. [[CrossRef](#)]



21. Scheiner, S.; Michalczyk, M.; Zierkiewicz, W. Coordination of anions by noncovalently bonded  $\sigma$ -hole ligands. *Coord. Chem. Rev.* **2020**, *405*, 213136. [\[CrossRef\]](#)
22. Alkorta, I.; Elguero, J.; Frontera, A. Not Only Hydrogen Bonds: Other Noncovalent Interactions. *Crystals* **2020**, *10*, 180. [\[CrossRef\]](#)
23. Gomilla, R.M.; Frontera, A. Charge assisted halogen and pnictogen bonds: Insights from the Cambridge Structural Database and DFT calculations. *CrystEngComm* **2020**. [\[CrossRef\]](#)
24. Zhao, Y.H.; Xu, H.B.; Fu, Y.M.; Shao, K.Z.; Yang, S.Y.; Su, Z.M.; Hao, X.R.; Zhu, D.X.; Wang, E.B. A Series of Lead(II)-Organic Frameworks Based on Pyridyl Carboxylate Acid N-Oxide Derivatives: Syntheses, Structures, and Luminescent Properties. *Cryst. Growth Des.* **2008**, *8*, 3566–3576. [\[CrossRef\]](#)
25. Wang, X.L.; Chen, Y.Q.; Gao, Q.; Lin, H.Y.; Liu, G.C.; Zhang, J.X.; Tian, A.X. Coordination Behavior of 5,6-Substituted 1,10-Phenanthroline Derivatives and Structural Diversities by Coligands in the Construction of Lead(II) Complexes. *Cryst. Growth Des.* **2010**, *10*, 2174–2184. [\[CrossRef\]](#)
26. Wibowo, A.C.; Vaughn, S.A.; Smith, M.D.; zur Loye, H.C. Novel Bismuth and Lead Coordination Polymers Synthesized with Pyridine-2,5-Dicarboxylates: Two Single Component “White” Light Emitting Phosphors. *Inorg. Chem.* **2010**, *49*, 11001–11008. [\[CrossRef\]](#)
27. He, J.; Zeller, M.; Hunter, A.D.; Xu, Z. White Light Emission and Second Harmonic Generation from Secondary Group Participation (SGP) in a Coordination Network. *J. Am. Chem. Soc.* **2012**, *134*, 1553–1559. [\[CrossRef\]](#)
28. Imran, M.; Mix, A.; Neumann, B.; Stammeler, H.G.; Monkowius, U.; Gründlinger, P.; Mitzel, N.W. Hemi- and holo-directed lead(II) complexes in a soft ligand environment. *Dalton Trans.* **2015**, *44*, 924–937. [\[CrossRef\]](#)
29. Mirdya, S.; Roy, S.; Chatterjee, S.; Bauzá, A.; Frontera, A.; Chattopadhyay, S. Importance of  $\pi$ -Interactions Involving Chelate Rings in Addition to the Tetrel Bonds in Crystal Engineering: A Combined Experimental and Theoretical Study on a Series of Hemi- and Holodirected Nickel(II)/Lead(II) Complexes. *Cryst. Growth Des.* **2019**, *19*, 5869–5881. [\[CrossRef\]](#)
30. Mirdya, S.; Banerjee, S.; Chattopadhyay, S. An insight into the non-covalent Pb...S and S...S interactions in the solid-state structure of a hemidirected lead(II) complex. *Cryst. Eng. Comm.* **2020**, *22*, 237–247. [\[CrossRef\]](#)
31. Tan, Y.-X.; Meng, F.-Y.; Wu, M.-C.; Zeng, M.-H. Two Pb(II) dicarboxylates constructed by rigid terephthalate or flexible D(+)-camphorate with different 3D motif based on cooperative effect of steric hindrance of ligand and lone pair electrons. *J. Mol. Struct.* **2009**, *928*, 176–181. [\[CrossRef\]](#)
32. Servati, G.M.; Stilinović, V.; Bauzá, A.; Frontera, A.; McArdle, P.; Van Derveer, D.; Ng, S.W.; Mahmoudi, G. Design of Lead(II) Metal-Organic Frameworks Based on Covalent and Tetrel Bonding. *Chem. Eur. J.* **2015**, *21*, 17951–17958. [\[CrossRef\]](#) [\[PubMed\]](#)
33. Mahmoudi, G.; Bauzá, A.; Frontera, A.; Garczarek, P.; Stilinović, V.; Kirillov, A.M.; Kennedy, A.; Ruiz-Pérez, C. Metal-organic and supramolecular lead(II) networks assembled from isomeric nicotinoylhydrazone blocks: The effects of ligand geometry and counter-ion on topology and supramolecular assembly. *CrystEngComm* **2016**, *18*, 5375–5385. [\[CrossRef\]](#)
34. Mahmoudi, G.; Bauzá, A.; Frontera, A. Concurrent agostic and tetrel bonding interactions in lead(II) complexes with an isonicotinohydrazide based ligand and several anions. *Dalton Trans.* **2016**, *45*, 4965–4969. [\[CrossRef\]](#)
35. Mahmoudi, G.; Bauza, A.; Amini, M.; Molins, E.; Mague, J.T.; Frontera, A. On the importance of tetrel bonding interactions in lead(II) complexes with (iso)nicotinohydrazide based ligands and several anions. *Dalton Trans.* **2016**, *45*, 10708–10716. [\[CrossRef\]](#) [\[PubMed\]](#)
36. Mahmoudi, G.; Dey, L.; Chowdhury, H.; Bauzá, A.; Ghosh, B.K.; Kirillov, A.M.; Seth, S.K.; Gurbanov, A.V.; Frontera, A. Synthesis and crystal structures of three new lead(II) isonicotinoylhydrazone derivatives: Anion controlled nuclearity and dimensionality. *Inorg. Chim. Acta* **2017**, *461*, 192–205. [\[CrossRef\]](#)
37. Mahmoudi, G.; Safin, D.A.; Mitoraj, M.P.; Amini, M.; Kubicki, M.; Doert, T.; Locherere, F.; Fleck, M. Anion-driven tetrel bond-induced engineering of lead(II) architectures with *N'*-(1-(2-pyridyl)ethylidene)nicotinohydrazide: Experimental and theoretical findings. *Inorg. Chem. Front.* **2017**, *4*, 171–182. [\[CrossRef\]](#)
38. Mahmoudi, G.; Gurbanov, A.V.; Hemida, S.R.; Corballo, R.; Amini, M.; Bacchi, A.; Mitoraj, M.P.; Sagan, F.; Kukulka, M.; Safin, D.A. Ligand-Driven Coordination Sphere-Induced Engineering of Hybride Materials Constructed from PbCl<sub>2</sub> and Bis-Pyridyl Organic Linkers for Single-Component Light-Emitting Phosphors. *Inorg. Chem.* **2017**, *56*, 9698–9709. [\[CrossRef\]](#) [\[PubMed\]](#)

39. Mahmoudi, G.; Zangrando, E.; Mitoraj, M.P.; Gurbanov, A.V.; Zubkov, F.I.; Moosavifar, M.; Konyaeva, I.A.; Kirillov, A.M.; Safin, D.A. Extended lead(II) architectures engineered via tetrel bonding interactions. *New J. Chem.* **2018**, *42*, 4959–4971. [\[CrossRef\]](#)
40. Seth, S.K.; Bauzá, A.; Mahmoudi, G.; Stilinović, V.; López-Torres, E.; Zaragoza, G.; Keramidas, A.D.; Frontera, A. On the importance of Pb···X (X = O, N, S, Br) tetrel bonding interactions in a series of tetra- and hexa-coordinated Pb(II) compounds. *CrystEngComm* **2018**, *20*, 5033–5044. [\[CrossRef\]](#)
41. Afkhami, F.A.; Mahmoudi, G.; Qu, F.; Gupta, A.; Köse, M.; Zangrando, E.; Zubkov, F.I.; Alkorta, I.; Safin, D.A. Supramolecular lead(II) architectures engineered by tetrel bonds. *CrystEngComm* **2020**, *22*, 2389–2396. [\[CrossRef\]](#)
42. Afkhami, F.A.; Mahmoudi, G.; Qu, F.; Gupta, A.; Zangrando, E.; Frontera, A.; Safin, D.A. Supramolecular architecture constructed from the hemidirected lead(II) complex with N'-(4-hydroxybenzylidene)isonicotinohydrazide. *Inorg. Chim. Acta* **2020**, *502*, 119350. [\[CrossRef\]](#)
43. Addison, A.W.; Nageswara, R.T.; Reedijk, J.; Van Rijn, J.; Verschoor, G.J. Synthesis, structure, and spectroscopic properties of copper(II) compounds containing nitrogen–sulphur donor ligands; the crystal and molecular structure of aqua[1,7-bis(N-methylbenzimidazol-2'-yl)-2,6-dithiaheptane]copper(II) perchlorate. *J. Chem. Soc. Dalton Trans.* **1984**, 1349–1356. [\[CrossRef\]](#)
44. Stroz, K. Plane groups—From basic to advanced crystallographic concepts. *Z. Kristallogr.* **2003**, *218*, 642–649.
45. Spackman, M.A.; Jayatilaka, D. Hirshfeld surface analysis. *CrystEngComm* **2009**, *11*, 19–32. [\[CrossRef\]](#)
46. Spackman, M.A.; McKinnon, J.J. Fingerprinting intermolecular interactions in molecular crystals. *CrystEngComm* **2002**, *4*, 378–392. [\[CrossRef\]](#)
47. Wolff, S.K.; Grimwood, D.J.; McKinnon, J.J.; Turner, M.J.; Jayatilaka, D.; Spackman, M.A. *CrystalExplorer 3.1*; University of Western Australia: Crawley, WA, Australia, 2012.
48. Jelsch, C.; Ejsmont, K.; Huder, L. The enrichment ratio of atomic contacts in crystals, an indicator derived from the Hirshfeld surface analysis. *IUCrJ* **2014**, *1*, 119–128. [\[CrossRef\]](#)
49. Safin, D.A.; Mitoraj, M.P.; Robeyns, K.; Filinchuk, Y.; Vande Velde, C.M.L. Luminescent mononuclear mixed ligand complexes of copper(I) with 5-phenyl-2,2'-bipyridine and triphenylphosphine. *Dalton Trans.* **2015**, *44*, 16824–16832. [\[CrossRef\]](#)
50. Babashkina, M.G.; Robeyns, K.; Filinchuk, Y.; Safin, D.A. Detailed studies of the interaction of 3-chloroaniline with O,O'-diphenylphosphorylthiocyanate. *New J. Chem.* **2016**, *40*, 1230–1236. [\[CrossRef\]](#)
51. Safin, D.A.; Vande Velde, C.M.L.; Babashkina, M.G.; Robeyns, K.; Filinchuk, Y. Mononuclear heteroleptic complexes of copper(I) with 5-phenyl-2,2'-bipyridine and triphenylphosphine: Crystal structures, Hirshfeld surface analysis and luminescence properties. *New J. Chem.* **2016**, *40*, 6156–6163. [\[CrossRef\]](#)
52. Safin, D.A.; Robeyns, K.; Babashkina, M.G.; Filinchuk, Y.; Rotaru, A.; Jureschi, C.; Mitoraj, M.P.; Hooper, J.; Brela, M.; Garcia, Y. Polymorphism driven optical properties of an anil dye. *CrystEngComm* **2016**, *18*, 7249–7259. [\[CrossRef\]](#)
53. Safin, D.A.; Robeyns, K.; Garcia, Y. 1,2,4-Triazole-based molecular switches: Crystal structures, Hirshfeld surface analysis and optical properties. *CrystEngComm* **2016**, *18*, 7284–7296. [\[CrossRef\]](#)
54. Safin, D.A.; Babashkina, M.G.; Mitoraj, M.P.; Kubisiak, P.; Robeyns, K.; Bolte, M.; Garcia, Y. An intermolecular pyrene excimer in the pyrene-labeled N-thiophosphorylated thiourea and its nickel(II) complex. *Inorg. Chem. Front.* **2016**, *3*, 1419–1431. [\[CrossRef\]](#)
55. APEX3, SAINT; v6.28A; Bruker AXS Inc.: Madison, WI, USA, 2016.
56. Sheldrick, G.M. SHELXT—Integrated space-group and crystal-structure determination. *Acta Crystallogr. Sect. C* **2015**, *71*, 3–8. [\[CrossRef\]](#) [\[PubMed\]](#)
57. Farrugia, L.J. WinGX and ORTEP for Windows: An update. *J. Appl. Cryst.* **2012**, *45*, 849–854. [\[CrossRef\]](#)
58. Frisch, M.J.; Trucks, G.W.; Schlegel, H.B.; Scuseria, G.E.; Robb, M.A.; Cheeseman, J.R.; Scalmani, G.; Barone, V.; Petersson, G.A.; Nakatsuji, H.; et al. *Gaussian 16, Revision A.03*; Gaussian, Inc.: Wallingford, CT, USA, 2016.
59. Adamo, C.; Barone, V. Toward reliable density functional methods without adjustable parameters: The PBE0 model. *J. Chem. Phys.* **1999**, *110*, 6158–6169. [\[CrossRef\]](#)
60. Grimme, S.; Antony, J.; Ehrlich, S.; Krieg, H. A dispersion correction for density functionals, Hartree-Fock and semi-empirical quantum chemical methods DFT-D3. *J. Chem. Phys.* **2010**, *132*, 154104. [\[CrossRef\]](#)
61. Weigend, F.; Ahlrichs, R. Balanced basis sets of split valence, triple zeta valence and quadruple zeta valence quality for H to Rn: Design and assessment of accuracy. *Phys. Chem. Chem. Phys.* **2005**, *7*, 3297–3305. [\[CrossRef\]](#)

62. Weigend, F. Accurate Coulomb-fitting basis sets for H to Rn. *Phys. Chem. Chem. Phys.* **2006**, *8*, 1057–1065. [[CrossRef](#)]
63. Bader, R.F.W. A quantum theory of molecular structure and its applications. *Chem. Rev.* **1991**, *91*, 893–928. [[CrossRef](#)]
64. Keith, T.A. *AIMAll*; Version 19.10.12; TK Gristmill Software: Overland Park, KS, USA, 2019.

**Sample Availability:** Samples of the compound  $[\text{PbL}(\text{NO}_2)]_n$  are available from the authors.



© 2020 by the authors. Licensee MDPI, Basel, Switzerland. This article is an open access article distributed under the terms and conditions of the Creative Commons Attribution (CC BY) license (<http://creativecommons.org/licenses/by/4.0/>).